

Eddy Current Brakes for Haptic Interfaces: Design, Identification, and Control

Andrew H. C. Gosline, *Student Member, IEEE*, and Vincent Hayward, *Fellow, IEEE*,

Abstract—We describe the design of an eddy current brake for use as programmable viscous damper for haptic interfaces. Unlike other types of programmable brakes, eddy current brakes can provide linear, programmable physical damping that can be modulated at high frequency. These properties makes them well suited as dissipative actuators for haptic interfaces. We overview the governing physical relationships, and describe design optimization for inertial constraints. A prototype haptic interface is described, and experimental results are shown that illustrate the improvement in stability when simulating a stiff wall that is made possible using programmable eddy current dampers.

Index Terms—Eddy current brake, haptic rendering, passivity control

I. INTRODUCTION

HAPTIC interface technology is a growing field of research in science and engineering. With demand for haptic interfaces in areas such as medical training, manufacturing, and perception research, the desire for high fidelity haptic interfaces continues to increase. The haptic interface hardware and control software play an important role in the fidelity of the interaction that a user can experience. A common desired property in the design and analysis of haptic interfaces is system passivity because it applies to linear and nonlinear systems alike [1]. Because interactive environments, whether they be teleoperated or virtual, exhibit nonlinear behavior, passivity is a useful framework to analyze haptic interfaces [2], [3].

Colgate and Schenkel use elegant theory to produce a fundamental relationship for passivity of a haptic wall rendering based on the virtual stiffness, update rate, virtual damping, and physical damping [4]. For clarification, physical damping refers to the inherent dissipation of an electromechanical device. Virtual damping, however, is defined as a dissipative term that is computed using a velocity estimation and output using the actuators of a haptic interface. It is clear from their result that physical damping is required for the force feedback system to be passive. More recently, Abbot and Okamura and others improved upon prior findings and developed a more general passivity relationship including contributions from sensor quantization and coulomb friction [5]–[7].

Manuscript submitted July 20, 2007, revised June 24, 2008, accepted August 8, 2008. This paper was presented in part at the World Haptics 2007 Conference (Second Joint Eurohaptics Conference And Symposium On Haptic Interfaces For Virtual Environment And Teleoperator Systems), Tsukuba, Japan, March 2007.

Andrew H. C. Gosline and Vincent Hayward are with the Department of Electrical and Computer Engineering, McGill University, Montréal, Canada (e-mail:hayward@cim.mcgill.ca)

Haptic interfaces use actuators, such as electric motors, to drive a linkage and deliver forces to the user. Typically, the complex electro-mechanical devices are controlled by a digital computer at a fixed sampling frequency. Because of the delay associated with discrete-time control, haptic interfaces are prone to limit cycles when physical dissipation is not sufficient. In most devices, in fact, dissipation is an accidental by-product of their design and is not controllable. In addition, uncertain dissipation arises from various origins such as dry friction, viscosity, or magnetic drag in the drives or in their torque amplification/transmissions mechanisms such as capstan drives.

Recently, researchers have investigated the use of dissipative actuators in haptic devices. An and Kwon describe a 1-DOF hybrid interface that uses a magnetorheological fluid brake in parallel with a DC motor [8], [9]. Similarly, Kwon and Song describe a 2-DOF hybrid haptic interface, using magnetorheological brakes and DC motors, based upon the Pantograph design [10]. These authors reported improved stability characteristics, and a higher achievable impedance when utilizing brakes. The characteristics of the brakes, however, limit the fidelity of the rendering. Brakes that involve contact between moving surfaces, or with particles in suspension, can be slow to actuate, and when they rely on particle magnetization, suffer from demagnetization hysteresis [11]. Moreover, by the nature of the physics used to create dissipation, all contact-based actuated brakes, including friction brakes [12], particle brakes [12], magnetorheological (MR) brakes [13], electrorheological (ER) brakes [14], exhibit nonlinear and often multi-valued relationships between velocity and braking torque, requiring compensation [15].

In an alternate approach, Mehling *et al.* take advantage of the dissipative properties of a DC motor by shunting the terminals with a resistor and capacitor in series to create frequency dependent electrical damping [16]. With this approach, the damping is not controllable, and is limited both by the magnitude of the back-EMF characteristics of the motor and the variability of the brush-collector contact resistance. Recently, the same group achieved a moderate increase of programmable electrical damping using a single motor winding of a brushless motor and a custom-designed analog feedback circuit to cancel the internal resistance of the winding [17]. To circumvent the complexities that arise from commutation, they restricted the range of motion to approximately 17° in their single DOF haptic interface [18].

Take for example a motor frequently used in haptic devices (model RE25, 18 V, Maxon Motors ag, Sachseln, Switzerland). The torque constant is $k = 16.3 \text{ mN}\cdot\text{m}\cdot\text{A}^{-1}$ which is also the

back-EMF constant expressed in $\text{V}\cdot\text{s}\cdot\text{rd}^{-1}$. The terminal resistance $R = 1.26 \Omega$. Shorting the terminals, the motor becomes a damper of coefficient $b = k^2/R = 0.21 \text{ mN}\cdot\text{m}\cdot\text{s}\cdot\text{rd}^{-1}$ which is at least one order of magnitude lower than that achieved by our prototype dampers. It is also the case that palpable transients are experienced each time coil commutation occurs. Transients are caused by sudden resistance changes resulting from the interaction of the brushes with discrete collector segments. Transients are also caused by the fact that different windings are inserted and removed from the circuit during commutation. In other words, at low velocities, the electrical dynamics of a DC motor cannot be approximated by a single RL circuit. This approximation is only valid, on average, at high velocities. For the accurate control of haptic interfaces, these dynamics need to be compensated by well-tuned wide-bandwidth current amplifiers. Similar observations apply to electronically commuted brushless motor designs.

In this paper, we propose the use of eddy current brakes (ECBs) as linear, fast actuating, programmable viscous dampers for haptic rendering. In Section II, the fundamentals of eddy current brake physics are presented and in Section III a single-number merit function is proposed that can concisely capture the performance of any given design. In Section IV, the design of an ECB brake is described. In Section V, experimental optimization of the damper blade to magnet pole geometry is discussed. In Section VII time-domain passivity control is described and implemented using ECBs retrofitted to a prototype haptic interface. Finally, Section IX gives concluding remarks and future recommendations.

II. EDDY CURRENT BRAKING

Eddy Current Brakes are magnetic devices simply described by a conductor that moves through a magnetic field. As a result of the motion, eddy currents — Foucault currents — are induced to create a resistive force that is proportional to the relative velocity, according Lorentz' Force Law. Although the phenomenon is difficult to analyze for complex geometries [19]–[21], the underlying relationship between angular velocity and torque can be derived with the help of several simplifying assumptions.

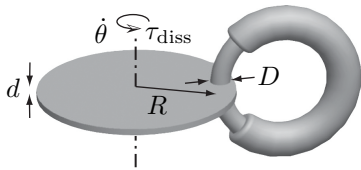


Fig. 1. Schematic Diagram of Eddy Current Brake

To familiarize readers with the underlying relationships, a simplified model from the literature is outlined. Following [22], and referring to Fig. 1, the induced current density in the conductor, J [$\text{A}\cdot\text{m}^{-2}$], is a function of the angular velocity, $\dot{\theta}$ [$\text{rd}\cdot\text{s}^{-1}$], the specific conductivity of the material, σ [$\Omega^{-1}\cdot\text{m}^{-1}$], the effective radius, R [m], and the magnetic field, B [T]:

$$|J| = \sigma R \dot{\theta} |B|. \quad (1)$$

Assuming that the magnetic flux is uniform through the air gap, and assuming that the conductive disc fits exactly within the air gap, the power dissipated by the eddy currents can be computed by integrating the currents over the cylindrical volume of the disc that is covered by the magnet pole:

$$P_{\text{diss}} = \frac{1}{\sigma} \int |J|^2 dV = \frac{\pi\sigma}{4} D^2 d B^2 R^2 \dot{\theta}^2, \quad (2)$$

where D [m] is the diameter of the magnet core. The braking torque, τ_{diss} [$\text{N}\cdot\text{m}$], is then:

$$\tau_{\text{diss}} = \frac{P_d}{\dot{\theta}} = \frac{\pi\sigma}{4} D^2 d B^2 R^2 \dot{\theta}. \quad (3)$$

According to (3), the drag torque should vary linearly with angular velocity. However, (1-3) are computed assuming that the applied magnetic field, B , is sufficiently greater than the magnetic field induced by the eddy currents. This assumption holds well at low speeds, and prior findings have shown that the braking force does vary linearly with velocity at low speeds [20], [21], [23]. Because haptic interfaces are designed for interaction with humans, the operating velocity of an interface is typically low, of the order of $200 \text{ mm}\cdot\text{s}^{-1}$ [24]. Conveniently, where eddy current braking is linearly dependent on velocity, the ECBs can be modeled as linear dampers that fit easily into robot kinematic/dynamic control frameworks.

III. MERIT FUNCTION

With a view to employ brakes in the design of haptic interface, it is natural to desire tradeoffs that maximize available damping for the smallest inertia. Hence, a crucial aspect of brake performance is captured by the ratio of these two quantities. Consider a damper with rotational inertia I [$\text{kg}\cdot\text{m}^2$] and damping coefficient b [$\text{N}\cdot\text{m}\cdot\text{s}\cdot\text{rd}^{-1}$]. Neglecting friction, the differential equation that describes its motion given an initial angular velocity, ω_0 , is:

$$\ddot{\theta} = -\frac{b}{I}\dot{\theta}, \quad \begin{cases} \theta(0) = 0, \\ \dot{\theta}(0) = \omega_0. \end{cases} \quad (4)$$

The angular velocity is

$$\dot{\theta}(t) = \omega_0 e^{-(b/I)t} = \omega_0 e^{-(1/\tau)t}, \quad (5)$$

therefore, the time constant $\tau = I/b$ [s] is an intrinsic characteristic of a design since it conveys its ability to reduce velocity.

IV. DESIGN OF AN EDDY CURRENT DAMPER FOR A PARALLEL HAPTIC INTERFACE

Several physical characteristics guide the design of an eddy current damper for a haptic interface. First, the inertia of the device should be kept to a minimum to allow for unrestricted free exploration [25]. Second, because stability is improved with added damping, the achievable damping should be maximized. Haptic interfaces have different damping and inertial requirements, whether they be serial or parallel, impedance or admittance based. In this paper, we focus on designing an eddy current damper for a common parallel linkage haptic interface named the Pantograph [26], [27].

The Pantograph is directly driven by two graphite brushed motors, model RE25 of Maxon Motors ag, located at the base of the device. The workspace generated by the 5-bar linkage restricts angular displacement to approximately 130 degrees. Because of this, it is relatively simple to retrofit ECB conductors to the proximal arms and make use of the free space available behind the device. Figure 2 shows prototype damping hardware retrofitted to a Pantograph interface. Annular aluminum sections are used, rather than disc sections, to reduce the rotating inertia. Each “damper blade” is actuated with an electromagnet driven by a current amplifier.

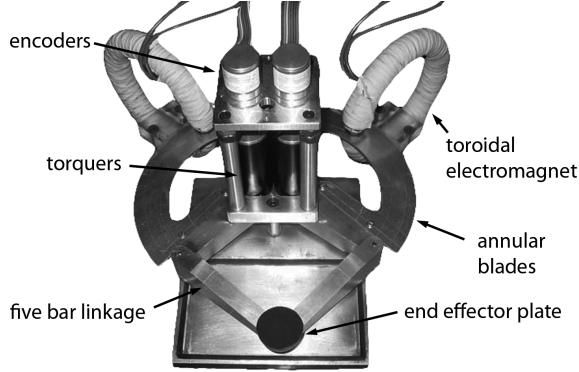


Fig. 2. Hybrid Pantograph with twin eddy current brakes.

To optimize the design of the damping hardware for minimal inertia and maximal damping, it is required to analyze the eddy current drag torque and rotational inertia. Note that while the damping torque scales quadratically with the effective radius, the inertia, I_{ann} [kg·m²], of an annulus also scales quadratically with the radius:

$$I_{\text{ann}} = \frac{1}{2} V_{\text{ann}} \rho (r_2^2 + r_1^2), \quad (6)$$

where V_{ann} [m³] is the volume of the annulus, ρ [kg·m⁻³] is the density of the annulus material, r_1 and r_2 [m] are the inner and outer radii respectively. It is important to note that the reluctance of the gap dominates the magnetic circuit, so the thickness of the annulus should remain small. Electromagnets are constructed with a toroidal core machined from soft iron and wrapped with 24 gage enamel coated copper wire. Toroidal magnet cores are known to provide an optimal magnetic path because there are neither sharp corners nor changes in cross section to leak magnetic flux.

Much of the prior engineering work with ECBs is focused towards the transportation industry for automotive and locomotive brakes [23], [28], [29]. In these applications, the inertia of the conductive disc has a relatively small impact on the overall inertia of the vehicle, and as such, materials such as iron and copper are acceptable. For a haptic interface, however, inertial constraints are important. The damper blade material must have both a low density for inertia reduction, and a high conductivity to promote the flow of eddy currents. According to (6), the inertia varies linearly with the density of the material, and according to (3), the damping varies linearly with the conductivity. These characteristics make electrical grade aluminum an excellent damper blade material as it has

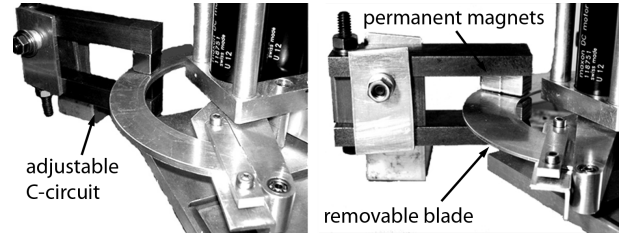


Fig. 3. Experimental apparatus showing two blade/magnet configurations out of the 32 combinations tested. The configuration on the left is a 3.18 mm thick, 12 mm wide blade with a single magnet pole. On the right is a 1.59 mm thick, 24 mm wide blade with two magnet poles in a radial arrangement.

the highest conductivity to density ratio of any conventional metal.

Having an optimal electromagnet design, and an optimal conductor material, the damper blade geometry and magnet pole geometry must be optimized for minimal inertia and maximal damping. In recent work, attempts to predict the influence of the finite boundary typical in rotary ECBs have shown limited success using either numerical or empirical simulation [21], [30], [31]. As such, experimental investigation of effect of the finite boundary was preferred over simulated analysis.

V. EXPERIMENTAL DAMPER BLADE AND MAGNETIC GEOMETRY OPTIMIZATION

In place of simulation, an experiment was set up to identify the optimal damper blade dimensions given practical physical constraints. Fig. 3 shows the experimental apparatus. Replaceable annular sections machined from standard thickness, 1.59 mm and 3.18 mm, electrical grade (Alloy 1100) aluminum sheet stock are attached to the base arm of the Pantograph with a shoulder flange and clamp. Rather than manufacture and wind several electromagnet cores, arrangements of permanent magnets are used to investigate the effect of magnet pole geometry in relation to the blade geometry.

A. Tests

An adjustable steel C-clamp magnetic circuit holds an array of 11 mm cubic-shaped rare earth magnets (NdFeB, Amazing Magnets LLC, Irvine, CA, USA) at a fixed tolerance gap away from the damper blade. The annular sections each have an effective radius of 50 mm, with widths w of 12, 16, 20, and 24 mm. As mentioned earlier, the width of the gap has influence on the magnetic field strength between the magnet poles. The field is approximately 1.0 T in the 1.59 mm blade configuration, and 0.9 T for the 3.18 mm blade as measured with a digital Gaussmeter (Model 1, AlphaLab Inc., Salt Lake City, UT, USA).

The system shown in Fig. 3 is modeled by:

$$I\ddot{\theta} + b\dot{\theta} + K\theta = \tau_{\text{fric}}(\theta), \quad (7)$$

where K [N·m·rd⁻¹] is a virtual spring programmed by the motor/encoder, I , is the inertia of the system, b , the viscosity from the ECB, and τ_{fric} is the friction from the bearings. To measure the damping coefficient of a given damper assembly,

an energy balance is considered between two rest states. In the first state, the deflected arm is loaded by a virtual spring with stiffness K_a through angle θ_a . At the second state, the arm has come to rest at, or near, the virtual spring's origin after release. This balance is first used to identify the energy loss due to friction over θ_a by:

$$E_{\text{fric}} = \frac{1}{2} K_a \theta_a^2 = \oint \tau_{\text{fric}}(\theta) d\theta, \quad (8)$$

where E_{fric} is the energy dissipated by friction over angle θ_a . If the arm moves from an the initial deflection, θ_a to the virtual spring's origin without overshooting, then all of the stored energy from the deflected spring is exactly dissipated by friction. In order to locate K_a such that the arm moves to its rest position without overshoot, a binary search method is employed. The procedure is stopped when the test succeeds four times to resist outliers. Once friction is quantified, a second virtual spring constant K_d is found such that the damped system travels over the same deflection without overshoot:

$$E(K_d) = E_d + E_{\text{fric}} = \int b \dot{\theta}(t) \dot{\theta}(t) dt + E_{\text{fric}}, \quad (9)$$

where $E(K_d)$ is the potential energy stored with the damped spring constant, E_d the energy dissipated by the damper, and E_{fric} the energy lost to friction from (8). Using the value of E_{fric} from (8), and solving for the damping coefficient:

$$b = \frac{\frac{1}{2} K_d \theta_a^2 - E_{\text{fric}}}{\int \dot{\theta}^2 dt}, \quad (10)$$

where $\int \dot{\theta}^2 dt$ is numerically integrated over θ_a . Control of the device is performed at a fixed update rate of 10 kHz on a 2.0 GHz PC running Linux kernel 2.6 and the Xenomai real-time framework. Input/Output is performed by a ISA digital acquisition board (Model II, Servo to Go, Inc., Indianapolis, IN, USA).

B. Experimental Results

For each damper blade, four different magnet arrangements are tested, as shown in Fig. 4. Arrangement using multiple permanent magnets are fastened together with fiberglass reinforced adhesive tape to counteract magnetic repellance of adjacent like-poles.

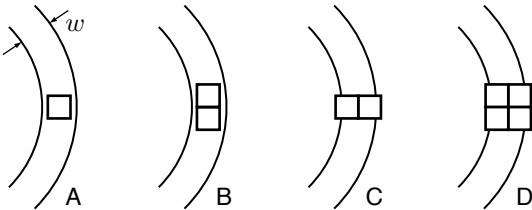


Fig. 4. Experimental magnet pole configurations: (A) single magnet, (B) double magnet tangential, (C) double magnet radial, (D) quad magnet.

Results from the experimental analysis are shown in Fig. 5. As expected, the physical boundary of the damper blade and its relationship with the magnet pole has a noticeable effect on the damping coefficient. The trends in Fig. 5 are

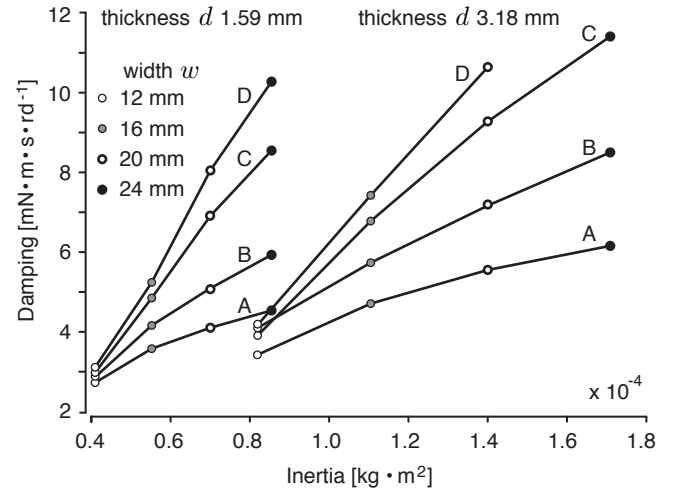


Fig. 5. Damping coefficient results.

consistent between the two thicknesses of damper blade. Also, it is important to note that doubling the thickness of the damper blade, from 1.59 mm to 3.18 mm corresponds to an improvement in damping of approximately 1.3 that is consistent among all cases. Twice the inertia for only a third more damping indicates that the blade should remain as thin as practically possible.

It is clear from Fig. 5 that the double magnet tangential case (B) is not an effective use of geometry, as the double magnet radial case (C) consistently improves the damping by a factor of 1.3 while maintaining the same magnet pole cross-sectional area and the same inertia. In fact, it is evident that an optimal magnet pole to blade geometry should completely shadow the blade width, as the double magnet radial and quad magnet cases do. Leaving any un-shadowed blade width is a poor use of inertia.

These findings are further supported by considering the data in Table I which shows the actuator rates of decay for each blade width and thickness for the case of a single magnet. It is clear from these results that the 1.59 mm damper blade provides superior performance to the 3.18 mm blade since the rate of velocity decay is much higher with the thinner blades. This is due to the stronger magnetic field present with a reduced air gap. The 12 mm wide, 1.59 mm thick blade provides the fastest velocity decay. This matches the conclusion that it is optimal to shadow as much of the blade width as possible with magnetic flux. The square poles have a width of approximately 11.1 mm, so the single magnet case is sufficient to almost completely shadow the width of the 12 mm wide blade. Though not shown, the rate of decay for the dual magnet configuration case (C) with the 12 mm wide blade is 73 s^{-1} , which shows that the rate is further improved by shadowing the remainder of the blade width.

There is some discrepancy in the results. The 12 mm wide blade has the highest rate of decay for a 1.59 mm thickness, while the 16 mm wide blade has the highest rate of decay for a 3.18 mm thickness. This can be explained by the fact that as the gap increases, the flux lines spread further apart. A blade that is slightly wider than the magnet pole will still be

TABLE I
RATES OF DECAY $1/\tau$ [s^{-1}] FOR THE SINGLE MAGNET CASE.

thickness (mm)	width (mm)			
	12	16	20	24
1.59	67	65	59	53
3.18	42	43	40	36

exposed to stray magnetic flux lines across all of its width.

Note that the experiments done in this section are aimed at an optimal damping to minimal inertia constraint, and no respect was paid to the power consumption of the electromagnets. In the tests, the electromagnets were replaced by permanent magnets for ease of experimentation. The design of an electromagnet is subject to similar tradeoffs, as the gage of wire, number of loops, thickness of air gap, and dimensions of the core all play a role in the performance of the electromagnet. Of larger concern, though, is the electronics that are required to actuate the electromagnets with sharp transients.

VI. ACTUATION OF ELECTROMAGNETS, AMPLIFIER SELECTION

The electrical characteristics of the electromagnet coil determine the bandwidth of the damper, which is of utmost importance for haptic rendering, as we need to actuate the end effector at high frequency to mask the discrete nature of the control loop. An electromagnet can be modeled as a resistor and an inductor in series, so the rate at which the damper can be turned on and off is a function of the inductance of the coil, L [H], the resistance, R [Ω], and the maximum transient voltage that the amplifier can supply, V_{cc} [V]. Voltage is related to current through:

$$v(t) = L \frac{di}{dt} + Ri. \quad (11)$$

In the Laplace domain, the transient response to a step input of voltage, corresponding to a turn-on command, is:

$$I(s) = \frac{V_{cc}}{s} \frac{1}{Ls + R}. \quad (12)$$

In the time domain, the step response is:

$$i(t) = \frac{V_{cc}}{R} \left(1 - e^{-L/Rt}\right). \quad (13)$$

Note that the inductance, L , appears only in the transient exponential, and that a higher V_{cc} will result in a faster turn-on time. Because we wish to maximize the frequency that the dampers can be actuated at, amplifiers should be chosen to maximize the driving voltage. Although it is desirable to have a large driving voltage for the transient response of an electromagnet, at steady state, the required voltage is quite low. As such, linear amplifiers are not suitable because they would be required to dissipate a large amount of power at steady state given a sufficiently large driving voltage. Pulse-width modulation (PWM) amplifiers, however, are capable of using a high driving voltage without dissipating large amounts of power at steady state. The only tradeoff is current ripple. The large electromagnets used in this work achieve inductance

that are at least ten times more than the minimum required inductance for the commercially available PWM amplifiers (AMC 20A20, Advanced Motion Controls, Camarillo, CA, USA) used in this work. Although no formal study was performed, the authors and several members of the laboratory concur that the current ripple from the PWM amplifiers creates neither tactually detectable mechanical noise nor perceivable acoustic noise.

VII. PASSIVITY BASED CONTROL WITH TUNABLE PHYSICAL DAMPERS

Passivity theory is a useful framework for analyzing control systems in general and haptic feedback in particular. Firstly, if a system is passive, it is globally stable in the sense that its free response always decays from any initial conditions. Secondly, if a complex system is broken down into several subsystems, the full system is passive if each subsystem is passive. This allows each subsystem to be investigated individually [1], [7]. All these properties are directly applicable to the design of mechanical virtual environments. Recently, rather than use passivity theory as a tool for analyzing control systems alone, it has been used in a real-time methodology to control haptic interfaces. Hannaford and Ryu developed a time-domain passivity control methodology that consists of two basic components, a passivity observer (PO), and a passivity controller (PC) [3]. Their method is briefly described to familiarize the readers with it.

A. Introduction to Time-Domain Passivity Control

A passive system is defined as one that cannot generate energy. In the control literature, a sign convention states that energy dissipation is positive. Following [3], a one port system with effort, f [N], flow, v [$m \cdot s^{-1}$], and initial energy storage, $E(0)$ [J], is passive if:

$$\int_0^t f(\tau)v(\tau)d\tau + E(0) \geq 0, \forall t \geq 0. \quad (14)$$

A Passivity Observer (PO) is an on-line numerical approximation of the energy flow in any portion of the interface or its control software. Assuming $E(0) = 0$, the PO is defined as:

$$E_{\text{obsv}}(n) = \Delta T \sum_{k=0}^n f(k)v(k), \quad (15)$$

where $E_{\text{obsv}}(n)$ is the approximate energy integral, ΔT (s) is the sampling period, $f(k)$ and $v(k)$ [$m \cdot s^{-1}$] are the k^{th} sample of force and velocity respectively. The equivalent expression using joint variables is:

$$E_{\text{obsv}}(n) = \Delta T \sum_{k=0}^n \tau(k)\omega(k), \quad (16)$$

where $\tau(k)$ and $\omega(k)$ are the k^{th} sample of torque and angular velocity respectively.

If the real-time value of either (15) or (16) becomes negative, this indicates that the observed portion of the energy flow is active, and the passivity controller (PC) is recruited. An impedance controlled haptic interface changes the force

displayed to the user based on the position of the manipulator. In the impedance configuration, a serially connected PC is used to modulate the discrete force output based on an input velocity. The first computation in the PC estimates a virtual damping coefficient that removes the active energy from the virtual environment using the update law:

$$\alpha(n) = \begin{cases} \frac{-E_{\text{obsv}}(n-1)}{\Delta T v(n)^2}, & \text{if } E_{\text{obsv}} < 0 \\ 0, & \text{if } E_{\text{obsv}} \geq 0 \end{cases}, \quad (17)$$

where $\alpha(n)$ [$\text{N}\cdot\text{s}\cdot\text{m}^{-1}$] is the virtual damping force coefficient. Due to the introduction of this virtual damping coefficient, the PO update law is modified to account for energy removed by damping:

$$E_{\text{obsv}}(n) = E_{\text{obsv}}(n-1) + \Delta T f_{\text{VE}}(n)v(n) + \Delta T \alpha(n-1)v(n-1)^2. \quad (18)$$

Applying the required virtual damping, the force output then becomes:

$$f_{\text{output}}(n) = f_{\text{VE}}(n) + \alpha(n)v(n), \quad (19)$$

where f_{VE} and f_{output} are the force computed by the virtual environment and force output to the actuators respectively.

Hannaford and Ryu's method maintains a passivity constraint by degrading system performance with additional virtual damping. In their work, the method was initially tested on the Excalibur Haptic Interface that is cable driven and exhibits considerable inherent friction [32]. More recently, their method has been applied to the popular PHANTOM haptic interface [33]. The authors needed to modify their technique by limiting the virtual damping to avoid exciting structural resonances in the PHANTOM. Enforcing a passivity constraint with virtual damping alone is not well suited, for two reasons, to devices that have minimal inherent dissipation, such as a direct drive Pantograph. First, because the control signal is dependent on a velocity estimation signal, it is necessary to limit the virtual damping to avoid over-amplification of a noisy velocity signal. For example, if a virtual damping coefficient of greater than approximately $2.5 \text{ N}\cdot\text{s}\cdot\text{m}^{-1}$ is used on the Pantograph, vibration is generated that is both audible and palpable despite the use of adaptive velocity estimation [34]. Second, at low velocity, the effect of the added virtual damping is minimal, and it is possible that insufficient physical dissipation could allow limit cycles near the boundary of a virtual wall.

In converting electrical energy to mechanical energy, DC motors are actually passive elements because the energy input is higher than energy output due to the impedance of the coils and friction. However, obtaining programmable dissipation from them is difficult because controlling the torque to oppose motion at all times can only be done to some approximation. In particular, time delay caused by sampling and reconstruction yields an erroneous signal each time the velocity changes sign. To make matters worse, steady state velocity can be known only to a velocity quantum δ/\mathcal{T} , where δ is the device resolution and \mathcal{T} the time window allocated to estimate velocity. It is possible to take advantage of known system dynamics and disturbance estimates to recover velocity

using signals other than position alone, but these methods are difficult to apply [35]. Rather than use actuators, such as DC motors, that were designed for purposes other than maintaining the passivity of a haptic interface, we demonstrate the use of programmable ECBs that were specifically designed for this end. Since ECBs are dissipative by nature, and can be actuated at high frequency, they are ideally suited to remove prescribed quantities of energy without time delay and without dependence on a velocity estimation signal.

B. Passivity Control with Physical Dampers

Hannaford and Ryu remove a prescribed amount of energy with virtual damping by:

$$E_{\text{diss}} = \alpha v(n-1)^2 \Delta T. \quad (20)$$

For the Pantograph with damped joints, it is more convenient to compute energy based on joint variables. Accordingly, (20) becomes:

$$E_{\text{diss}} = \beta \omega(n-1)^2 \Delta T \quad (21)$$

where β is the damping torque coefficient of a joint.

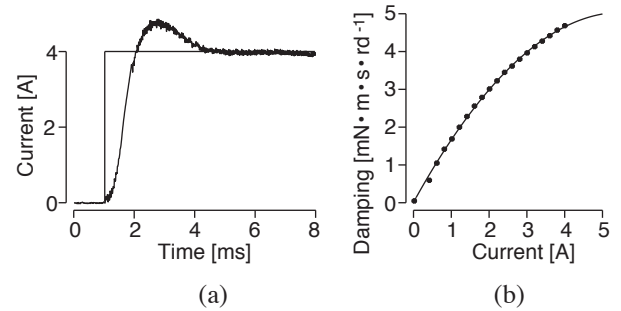


Fig. 6. ECB Actuation Properties. (a) Closed-loop step response to a 4 A current command. (b) Damping to coil current relationship.

Control of the damping coefficient requires that actuation and damping characteristics of the ECB dampers are known. According to Fig. 6, under closed loop control, the dampers have a finite actuation time and a nonlinear current to damping coefficient relationship. Because a fixed update frequency of 10 kHz is used to control the Pantograph, the dampers require multiple update periods to actuate, and their dynamics must be modeled and incorporated in the PC. Fig. 6(a) shows the coil current response to a 4 A step command, and illustrates the speed at which the ECBs can be actuated. Using a 180 V power supply, the amplifiers can drive the ECB coil current to 4 A in one millisecond. Accordingly, the ECB amplifier and coil combination can be modeled with a linear slew rate of approximately $4000 \text{ A}\cdot\text{s}^{-1}$. A quadratic least-squares fit approximates the damping coefficient to coil current relationship well, as shown in Fig. 6(b) The fit was found to be:

$$\beta = a i_{\text{coil}}^2 + b i_{\text{coil}} \quad (22)$$

where i_{coil} is the coil current (A), $a = -0.16$ and $b = 1.8$. The fact that damping coefficient curve levels off at approximately $5 \text{ mN}\cdot\text{m}\cdot\text{s}\cdot\text{rd}^{-1}$ is attributed to saturation effects in the iron core

of the magnet. The approximate response to a step command of current β becomes:

$$\beta = a(\text{SR } N \Delta T)^2 + b(\text{SR } N \Delta T) \quad (23)$$

where N is an integer that keeps track of the number of sampling periods expired since the dampers were activated and SR is the approximate slew rate of the amplifiers. Because the physical dampers are controlled in open loop, and cannot turn on completely in one time step, it is necessary to approximate the current state of the dampers. Approximating the coil current by $N \text{SR } \Delta T$ allows for a convenient method to approximate the present state of the dampers during transients.

The control loop for the ECB damper PC, including the necessary saturation to protect the coils from overheating, is calculated using the following algorithm.

- 1) Update the PO using the actual state of the dampers, β_a :

$$E_{\text{obsv}}(n) = E_{\text{obsv}}(n-1) + \Delta T \tau_{\text{VE}}(n) \omega(n) + \beta_a(n-1) \omega(n-1)^2 \Delta T. \quad (24)$$

- 2) Compute the desired damping β_d

$$\beta_d(n) = \begin{cases} \frac{-E_{\text{obsv}}(n-1)}{\Delta T \omega(n)^2}, & \text{if } (E_{\text{obsv}} < 0) \wedge (\beta_d < \beta_{\text{max}}) \\ \beta_{\text{max}}, & \text{if } (E_{\text{obsv}} < 0) \wedge (\beta_d > \beta_{\text{max}}) \\ 0, & \text{if } E_{\text{obsv}} \geq 0 \end{cases} \quad (25)$$

- 3) Damper actuation logic. Actual state of dampers, N_a :

- If $E_{\text{obsv}} < 0$ AND dampers off, set required current and set $N_a(n) = 1$.
- If $E_{\text{obsv}} < 0$ AND dampers on, set required current, then update N_a for next time step.

$$N_a(n) = \begin{cases} N_a(n-1) + 1, & \text{if } \beta_d > \text{SR } \Delta T N_a(n-1) \\ N_a(n-1) - 1, & \text{if } \beta_d < \text{SR } \Delta T N_a(n-1) \end{cases} \quad (26)$$

- Else if $E_{\text{obsv}} > 0$, turn dampers off and set $N_a(n) = 0$.

- 4) Update approximation of β_a using (23) with $\Delta T = 10^{-4}$ s, and $\text{SR} = 4000 \text{ A}\cdot\text{s}^{-1}$:

$$\beta_a(n) = \begin{cases} a(N_a(n) \text{SR } \Delta T)^2 + b(N_a(n) \text{SR } \Delta T), & \text{if } N_a(n) \leq N_{\text{sat}} \\ a(N_{\text{sat}} \text{SR } \Delta T)^2 + b(N_{\text{sat}} \text{SR } \Delta T), & \text{if } N_a(n) > N_{\text{sat}} \end{cases} \quad (27)$$

where N_{sat} is the number of time steps at SR to reach the overheating limit. For these experiments, the maximum allowable coil current was set to 4 A, hence $N_{\text{sat}} = 10$.

VIII. RESULTS

Experiments were performed to compare the performance of the virtually damped PC and the physically damped PC. For these experiments, a virtual wall located at $x = 0$, with $-x$ being inside the wall, was rendered with the Pantograph as shown in Fig. 7. The experiments were performed using the

same control hardware and real-time software architecture as described in Section V-A. Repeatable contact was simulated using a pre-tensioned elastic band to thrust and hold the manipulandum against the virtual wall. The elastic band allows us to closely examine the passivity characteristics of the device and control software without the fluctuating and highly dissipative properties of a human operator. Velocity estimation was computed using a previously described method with a window size of 16, and maximum number of outliers of 2 [34].



Fig. 7. Experimental Apparatus. The pre-tensioned elastic band allows repeatable wall contact with a passive operator.

Fig. 8 shows results using the virtually damped PC. Below each position trace is an energy trace, as computed by (15). Fig. 8(a) and 8(b), show results from an undamped $1.5 \text{ N}\cdot\text{mm}^{-1}$ virtual wall. This wall shows clear active behavior, as there is a stable limit cycle around $x = 0$, and the energy continues into the negative values over time. Figures 8(c) and 8(d) show results using the virtually damped PC with a $1.5 \text{ N}\cdot\text{mm}^{-1}$ wall. Note that the energy stays near the positive, yet there is still a limit cycle, of decreased magnitude and increased frequency, around $x = 0$, due to the delayed and noisy nature of virtual damping.

Fig. 9 shows results using the physically damped PC with a $1.5 \text{ N}\cdot\text{mm}^{-1}$ wall. The limit cycle that was present in both prior wall renderings is quenched with the addition of the physically damped PC. It is important to note that the slower response time of the physical dampers makes the negative energy spikes that correspond to each wall impact larger and longer than in the virtually damped case. Fig. 9(b,c) shows how the passivity controller must raise brake activation to saturation as the velocity decays in order to generate the required dissipation. This process continues until the system is completely at rest.

IX. CONCLUSION

The pertinent background to dissipative actuation and passivity control of haptic interfaces were first discussed to familiarize the reader with the focus of this paper. Basic eddy current brake physics were presented, the design of an ECB damper for the Pantograph haptic interface was described, and results from an experimental optimization of damping hardware were discussed. A prior existing time-domain passivity control methodology was adapted for the use of physical damping, rather than virtual. The physically damped passivity controller was shown to improve stability of virtual stiff wall. The authors would like to note that virtual walls rendered using the physical dampers do not have the characteristic “sticky” feel that is typical of walls

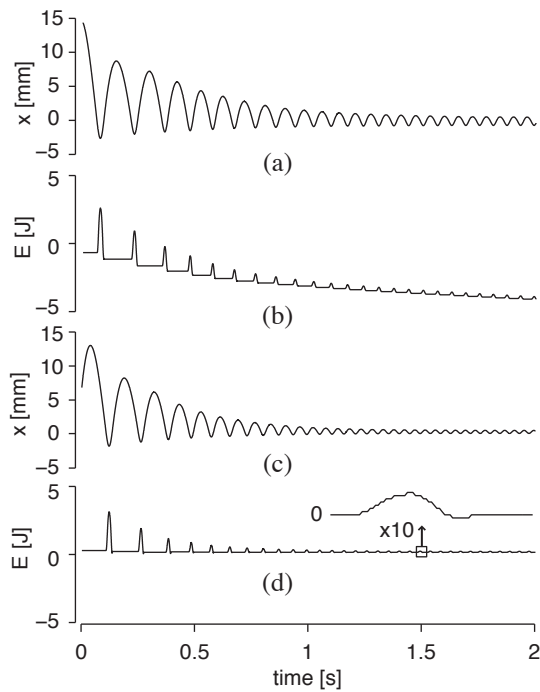


Fig. 8. Results using virtually damped passivity controller. Undamped $1.5 \text{ N}\cdot\text{mm}^{-1}$ virtual wall (a) and (b). Wall at $1.5 \text{ N}\cdot\text{mm}^{-1}$ with virtually damped Passivity Controller (c) and (d). The limit cycle is made more visible by enlargement in the bottom panel.

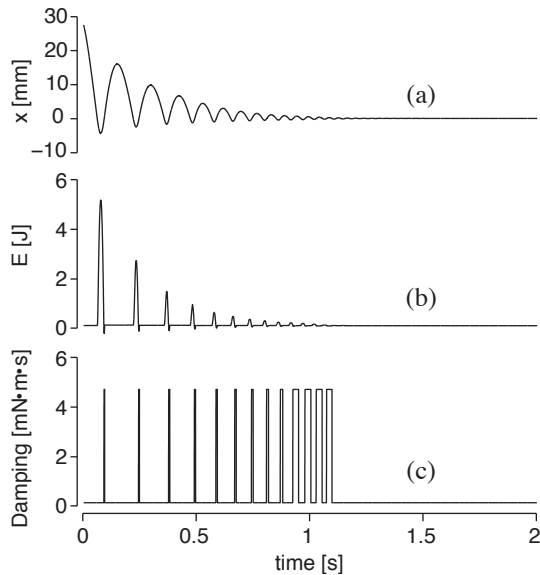


Fig. 9. Results using the physically damped passivity controller. Position (a). Energy (b). Damping coefficient (c).

rendered using conventional programmable brakes. This is due to both the fast dynamics of the ECB system (compared to commercially available MR brakes), and the fact that ECBs are linear and thus have a small effect at low speeds.

There are several limitations to the use of ECB dampers with a haptic interface. Despite efforts to minimize inertia, the additional damping hardware creates a noticeable increase in the inertia of the device. Second, as electromagnets are used to actuate the ECB dampers, the power consumption of the device

increases considerably. There are also limitations to the use of physical dampers for passivity control. First, as this method is dependent on additional hardware, a haptic interface would have to be equipped with programmable physical dampers to make use of this method. Second, as the dampers actuate slower than the motors, the system energy could be in the active region longer than if virtual damping was used.

The use of ECB dampers for haptic rendering has shown promising results, yet this work leaves an open door to a myriad of future research projects. To name a few:

- Design: ECB dampers have been retrofit to an existing haptic interface, yet to extend this work to other interfaces, a more compact design is likely necessary. A good target is creating an ECB damper that has a similar form factor to a MR brake.
- Devices: Because of their intrinsic qualities for control, ECB dampers could be applied to the design of all-passive haptic interfaces [36], [37].
- Teleoperation: The benefits of using dissipative hardware in passivity control should also be investigated for teleoperation. As dissipative hardware does not suffer from the actuation problems associated with time delay, it could be used to provide high fidelity master arm control.
- Motion Control: Because ECB dampers can be actuated at high frequency, and have excellent stability characteristic they would likely be valuable additions to general purpose motion control or high performance robotics.

ACKNOWLEDGMENT

This work was funded by a Collaborative Research and Development Grant “High Fidelity Surgical Simulation” from NSERC, the Natural Sciences and Engineering Council of Canada and by Immersion Corp., and by a Discovery Grant also from NSERC. The authors would also like to thank Guillaume Millet and the reviewers for their insightful comments and criticisms.

REFERENCES

- [1] R. J. Anderson and M. W. Spong, “Bilateral control of teleoperators with time delay,” *IEEE Transactions on Robotics and Automation*, vol. 34, no. 5, pp. 494–501, 1989.
- [2] G. Niemeyer and J.-J. Slotine, “Stable adaptive teleoperation,” *IEEE Journal of Oceanic Engineering*, vol. 16, no. 1, pp. 152–162, 1991.
- [3] B. Hannaford and J. H. Ryu, “Time-domain passivity control of haptic interfaces,” *IEEE Transactions on Robotics and Automation*, vol. 18, no. 1, pp. 1–10, 2002.
- [4] J. E. Colgate and G. Schenkel, “Passivity of a class of sampled-data systems: Application to haptic interfaces,” in *Proceedings of the American Control Conference*, 1994, pp. 3236–3240.
- [5] J. J. Abbott and A. M. Okamura, “Effects of position quantization and sampling rate on virtual wall passivity,” *IEEE Transactions on Robotics*, vol. 21, no. 5, pp. 952–964, 2005.
- [6] N. Diolaiti, G. Niemeyer, F. Barbagli, and J. K. Salisbury, “Stability of haptic rendering: Discretization, quantization, time delay, and coulomb effects,” *IEEE Transactions on Robotics*, vol. 22, no. 2, pp. 256–268, 2006.
- [7] M. Mahvash and V. Hayward, “High fidelity passive force reflecting virtual environments,” *IEEE Transactions on Robotics*, vol. 21, no. 1, pp. 38–46, 2005.
- [8] J. An and D. S. Kwon, “Stability and performance of haptic interfaces with active/passive actuators theory and experiments,” *International Journal of Robotics Research*, vol. 25, no. 11, pp. 1121–1136, 2006.

- [9] —, “Control of multiple dof hybrid haptic interface with active/passive actuators,” in *IEEE/RSJ International Conference in Intelligent Robots and Systems IROS’05*, 2005, pp. 2572–2577.
- [10] T. B. Kwon and J. B. Song, “Force display using a hybrid haptic device composed of motors and brakes,” *Mechatronics*, vol. 16, pp. 249–257, 2006.
- [11] C. L. Kapuscinski, “Motor selection and damper design for a six degree of freedom haptic display,” Master’s thesis, Department of Mechanical Engineering, Northwestern University, 1997.
- [12] M. Gogola and M. Goldfarb, “Design of a PZT-actuated proportional drum brake,” *IEEE Transactions on Mechatronics*, vol. 4, no. 4, pp. 409–416, 1999.
- [13] J. Lozada, M. Hafez, and X. Boutillon, “A novel haptic interface for musical keyboards,” in *IEEE/ASME International Conference on Advanced Intelligent Mechatronics*, Sept. 2007, pp. 1–6.
- [14] T. Nakamura and N. Saga, “Viscous control of homogeneous ER fluid using a variable structure control,” *IEEE/ASME Transactions on Mechatronics*, vol. 10, no. 2, pp. 154–160, 2005.
- [15] A. Milecki, “Investigation and control of magneto-rheological fluid dampers investigation and control of magneto-rheological fluid dampers investigation and control of magneto-rheological fluid dampers,” *International Journal of Machine Tools & Manufacture*, vol. 41, pp. 379–391, 2001.
- [16] J. S. Mehling, J. E. Colgate, and M. A. Peshkin, “Increasing the impedance range of a haptic display by adding electrical damping,” in *Proceedings of the First Joint Eurohaptics Conference and Symposium on Haptic Interfaces for Virtual Environment and Teleoperator Systems, World Haptics 2005*, 2005, pp. 257–262.
- [17] D. W. Weir, J. E. Colgate, and M. A. Peshkin, “Measuring and increasing Z-width with active electrical damping,” in *Proceedings of the Symposium on haptic interfaces for virtual environment and teleoperator systems*, 2008, pp. 169–175.
- [18] D. W. Weir, M. A. Peshkin, J. E. Colgate, and P. Buttolo, “Design and performance of a high fidelity, low mass, linear haptic display,” in *Proceedings of the First Joint Eurohaptics Conference and Symposium on Haptic Interfaces for Virtual Environment and Teleoperator Systems, World Haptics*, 2005, pp. 177–182.
- [19] H. D. Wiederick, H. Gauthier, D. A. Campbell, and P. Rochon, “Magnetic braking: Simple theory and experiment,” *American Journal of Physics*, vol. 55, no. 6, pp. 500–503, 1987.
- [20] M. A. Heald, “Magnetic braking: Improved theory,” *American Journal of Physics*, vol. 56, no. 6, pp. 521–522, 1988.
- [21] K. Lee and K. Park, “Modeling eddy currents with boundary conditions by sing coulomb’s law and the method of images,” *IEEE Transactions on Magnetics*, vol. 38, no. 2, pp. 1333–1340, 2002.
- [22] E. Simeu and D. Georges, “Modeling and control of an eddy current brake,” *Control Engineering Practise*, vol. 4, no. 1, pp. 19–26, 1996.
- [23] S. Anwar, “A parametric model of an eddy current electric machine for automotive braking applications,” *IEEE Transactions on Control Systems Technology*, vol. 12, no. 3, pp. 422–427, 2002.
- [24] S. J. Lederman, R. L. Klatzky, C. L. Hamilton, and G. I. Ramsay, “Perceiving roughness via a rigid probe: Psychophysical effects of exploration speed and mode of touch,” *Haptics-E: Electronic Journal of Haptics Research*, vol. 1, 1999.
- [25] V. Hayward and O. R. Astley, “Performance measures for haptic interfaces,” in *Robotics Research: The 7th International Symposium*, G. Giralt and G. Hirzinger, Eds. Heidelberg: Springer Verlag, 1996, pp. 195–207.
- [26] C. Ramstein and V. Hayward, “The pantograph: A large workspace haptic device for a multi-modal human-computer interaction,” in *Proceedings of the SIGCHI conference on Human factors in computing systems, CHI’04, ACM/SIGCHI Companion-4/94*, 1994, pp. 57–58.
- [27] G. Champion, Q. Wang, and V. Hayward, “The Pantograph Mk-II: A haptic instrument,” in *Proceedings of the IEEE/RSJ International Conference on Intelligent Robots and Systems, IROS’05*, 2005, pp. 723–728.
- [28] S. E. Gay and M. Ehsani, “Parametric analysis of eddy -current brake performance by 3-d finite-element analysis,” *IEEE Transactions on Magnetics*, vol. 42, no. 2, pp. 319–328, 2006.
- [29] K. Lee and K. Park, “Optimal robust control of a contactless brake system using an eddy current,” *Mechatronics*, vol. 9, pp. 615–631, 1999.
- [30] S. E. Gay and M. Ehsani, “Analysis and experimental testing of a permanent magnet eddy-current brake,” in *Proceedings of the 2005 IEEE Conference on Vehicle Power and Propulsion*, 2005, pp. 756–765.
- [31] K. Lee and K. Park, “Analysis of an eddy-current brake considering finite radius and induced magnetic flux,” *Journal of Applied Physics*, vol. 92, no. 9, pp. 5532–5538, 2002.
- [32] R. J. Adams, M. Moreyra, and B. Hannaford, “Excalibur, a three-axis force display,” in *Proceedings ASME IMECE Symposium on Haptic Interfaces for Virtual Environments and Teleoperator Systems*, 1999.
- [33] J. H. Ryu, C. Preusche, B. Hannaford, and G. Hirzinger, “Time domain passivity control with reference energy following,” *IEEE Transactions on Control Systems Technology*, vol. 13, no. 5, pp. 737–742, 2005.
- [34] F. Janabi-Sharifi, V. Hayward, and C.-S. J. Chen, “Discrete-time adaptive windowing for velocity estimation,” *IEEE Transactions On Control Systems Technology*, vol. 8, no. 6, pp. 1003–1009, 2000.
- [35] P. R. Bélanger, “Estimation of Angular Velocity and Acceleration from Shaft Encoder Measurements,” in *Proceedings of IEEE International Conference on Robotics and Automation*, 1992, pp. 585–592.
- [36] C. Cho, J.-B. Song, and M. Kim, “Energy-based control of a haptic device using brakes,” *IEEE Transactions on Systems, Man, and Cybernetics—Part B: Cybernetics*, vol. 37, no. 2, pp. 341–349, 2007.
- [37] G. Champion, A. H. Gosline, and V. Hayward, “Passive viscous haptic textures,” in *Proceedings from Symposium on Haptic Interfaces For Virtual Environment And Teleoperator Systems*, 2008, pp. 379–380.



Andrew H.C. Gosline received his B.Sc in 2001 from Queen’s University in Mechanical Engineering. He then received his M.A.Sc in 2003 from the University of British Columbia in Electrical Engineering, studying with Tim Salcudean and Joseph Yan. Currently, Andrew is a PhD Candidate at McGill University in Electrical Engineering, studying with Vincent Hayward. His research interests include haptic interfaces, applied control, robotic actuation, medical simulation, and mechatronic systems design.



Vincent Hayward (M’84-SM’04-FIEEE’08), Ing. Ecole Centrale de Nantes 1978; Ph.D. Computer Science 1981, University of Paris; Visiting Assistant Professor, Purdue University (1982); Chargé de Recherches at CNRS, France (1983–86), Professeur invité, Université Pierre et Marie Curie (2006); is now Professor of Electrical and Computer Engineering at McGill University. Hayward is interested in haptic device design and applications, perception, and robotics. He is leading the Haptics Laboratory at McGill University and was the Director of the Center for Intelligent Machines (2001–2004). He is a co-Founder of the Experimental Robotics Symposia, Program Vice-Chair 1998 IEEE Conference on Robotics and Automation, Program Vice-Chair ISR2000, past Associate Editor of the IEEE Transactions on Robotics and Automation, now member of the Governing board of Haptics-e, of the Editorial board of the ACM Transactions on Applied Perception, and of the IEEE Transactions on Haptics. Hayward received best paper and research awards including the NASA Space Act Tech Brief Award (1991) and the E. (Ben) & Mary Hochhausen Award for Research in Adaptive Technology For Blind and Visually Impaired Persons (2002).